A SARS MULTIBAND SPECTRUM SENSING METHOD IN WIDEBAND COMMUNICATION SYSTEMS USING RSG

Bashar I. Ahmad, Andrzej Tarczynski and Mustafa Al-Ani

School of Electronics and Software Engineering, University of Westminster
115 New Cavendish Street, London W1W 6UW {email: bashar.ahmad@my.westminster.ac.uk; tarczya@westminster.ac.uk}

ABSTRACT

This paper introduces a multiband spectrum sensing method that can accomplish the sensing task using sampling rates considerably lower than the ones demanded by the uniform-sampling-based techniques. It utilises nonuniform sampling in conjunction with an appropriate spectral analysis tool. The approach is referred to as Spectral Analysis of Randomized Sampling (SARS), namely for the Random Sampling on Grid (RSG) scheme. The statistical characteristics of the adopted periodogram-type estimator are presented and the effects of the cyclostationary nature of the processed communication signals on SARS are addressed. Reliability guidelines that ensure the credibility of the sensing procedure amid a sought system performance are derived. Unlike a number of previously reported nonuniform sampling schemes e.g. Total Random Sampling (TRS), the RSG provides safeguards making it more suitable for implementation in hardware. Numerical examples testify the presented analytical results.

1. INTRODUCTION

Spectrum sensing involves scanning part(s) of the radio spectrum in search for a meaningful activity e.g. a transmission. The envisioned Cognitive Radio (CR) technology has initiated intensive research into effective spectrum sensing techniques [1, 2]. To perform the sensing task using uniform-sampling-based DSP without prior knowledge of the incoming signal's frequency support, the sampling rates should be at least twice the total monitored frequency range(s) regardless of the spectral activity within [3]. Otherwise aliasing would introduce irresolvable detection problems. In the event of examining wide bandwidths, such a constraint can pose a challenge to the system designer where high sampling rates and treating large quantities of data are required [1, 2, 4, 5]. Such stringent demands can be beyond the capability of the commercially available data acquisition devices i.e. Analogue to Digital Converters (ADCs).

In this paper, we proposed a method that can reliably sense the spectrum using an arbitrary low-rate nonuniform sampling and appropriate processing of the signal-a methodology known by Digital Alias-free Signal Processing (DASP) [6]. Operating at low sampling rates, can exploit the sensing device resources e.g. power more efficiently and/or evade the possible need for a specialized hardware. Here, the scenario where the overseen wide bandwidth consists of a number of disjoint spectral subbands is considered i.e. Multiband Spectrum Sensing (MSS). In such scenarios, MSS approaches that are based on nonparametric spectral analysis are viewed as adequate low-complexity options [1, 2]. A periodogram-type estimator, a tool that retained its popularity [1, 2], is deployed in this study for the SARS purpose.

Low rate tactful sampling and processing aimed at mitigating the aliasing/bandwidth limitation of uniform sampling has triggered an immense interest in the emerging Compressive Sensing (CS) trend e.g. [4, 5]. Reconstructing the sampled signal is inherently an integrated part of CS that imposes sampling frequencies above the Landua rate i.e. twice the effective bandwidth of the present signal not the monitored bandwidth. The difference between the latter two can be significant with low spectrum occupancy e.g. some CR systems. However, reconstruction might not be needed in certain tasks e.g. MSS. CS capability and performance comes at a considerable computational cost accompanying the optimisations it entails. Whilst the simplicity, low computational load and not having a lower limit on the utilised sampling rate are the main advantages of the proposed SARS method over CS or other approaches e.g. spectrum-blind sampling [7].

A SARS technique that relies on the TRS scheme was studied in [8]. Related work in the literature on MSS with SARS can be found therein. It was shown that MSS can be carried out with arbitrary low sampling rates. However, any two or more points of a TRS sequence can be arbitrarily close i.e. TRS requires infinitely fast ADC(s). Other randomised sampling schemes for DASP e.g. Poisson sampling suffer from a similar defect [6]. In this paper, an alternative sampling scheme, i.e. RSG, is adopted. It guarantees a minimum distance between any two sample points, requests lower sampling rates than TRS and is better suited for the use of FFT-like algorithms [9]. It is more practical and efficient. The statistical characteristics of SARS with RSG are presented here and the impact of the cyclostationary nature of communication signals is scrutinised. Unlike [8, 9], the nonstationarity of the processed signal is not circumvented – a widely adopted practice in the literature [1, 2]. It is shown to have repercussions especially on the SARS accuracy i.e. abrupt deterioration at certain frequency points. We provide guidelines to ensure that the MSS procedure meets the sought detection probabilities. The system subbands can have different power levels e.g. due to the propagation channel effect(s). This is distinct from [8, 9] where the surveyed subbands are assumed to be of equal power levels and a generic Chebychev's inequality parameter depicts the MSS performance.

2. MULTIBAND SPECTRUM SENISNG

2.1 System Model and Problem Formulation

The frequency range of interest encompasses L disjunct contiguous subbands each of width B_C i.e. the monitored

bandwidth $\mathcal{B}=[f_{in}, f_{in}+B]$ of a predefined f_{in} has a width $B=LB_C$. The incoming multiband signal at the sensing device is: $x(t)=\sum_{m=1}^{M} x_m(t)$ where M is the unknown number of the concurrently active subbands and $x_m(t)$ is the transmission corresponding to the m-th active subband. The samples of the zero mean wide sense cyclostationary signal $x(t)$ are contaminated with additive white Gaussian noise with variance P_N i.e. $y(t_n)=x(t_n)+n(t_n)$. Due to adverse system conditions e.g. propagation-channel effects, the individual transmissions $x_m(t)$'s can be of various power levels. Our objective in this study is to devise an algorithm that is capable of scanning the overseen bandwidth $\mathcal{B}$ and unveiling the active subbands. It should operate at rates significantly lower than the theoretical minimum permissible uniform sampling one $2B$ (not always achievable) [3].

Let $x_k(t)$ be the incoming linearly modulated continuous-time signal corresponding to one of the system subbands:

$$x_k(t)=\sum_{n=-\infty}^{+\infty} a_{n,k}\, s_{i,k}(t,n)+\sum_{n=-\infty}^{+\infty} b_{n,k}\, s_{q,k}(t,n). \quad (1)$$

The coefficients $\{a_{n,k}\}_{n\in\mathbb{Z}}$ and $\{b_{n,k}\}_{n\in\mathbb{Z}}$ are the transmitted symbols with variances $\sigma_{a,k}^2$ and $\sigma_{b,k}^2$ respectively. Whilst $s_{i,k}(t,n)=[p_{i,k}(t+nT_{S,k})\cos(2\pi f_{C,k}t)]\otimes h_k(t)$, $s_{q,k}(t,n)=[p_{q,k}(t+nT_{S,k})\cos(2\pi f_{C,k}t+0.5\pi)]\otimes h_k(t)$, $\otimes$ denotes the convolution operation and $h_k(t)$ is the propagation channel impulse response over the k-th subband with a central frequency $f_{C,k}$ and symbol rate $f_{S,k}=1/T_{S,k}$. Each of $p_{i,k}(t)$ and $p_{q,k}(t)$ are the baseband shaping filter(s) in the inphase and quadrature branches respectively.

2.2 Random Sampling on Grid

RSG scheme selects randomly N sampling instants inside an analysis time window $\mathcal{T}_r=[\mathcal{t}_r, \mathcal{t}_r+T_0]$. Let $\alpha=N/T_0$ denote the average sampling rate. The RSG samples are restricted to a specific finite set of time-instants that are equally spaced and placed within $\mathcal{T}_r$. They form an underlying uniform sampling grid whose sampling rate and total number of samples are given by $f_g=1/T_g$ and N_g respectively. Any of the grid points can be selected only once, i.e. without replacement, with equal probability where $C_N^{N_g}$ possible sampling sequences of length N exist.

2.3 Adopted Sensing Technique

The approach adopted here deploys a periodogram-type tool:

$$X_e(\mathcal{t}_r,f)=(N_g-1)T_0\left|\sum_{n=1}^{N} y(t_n)w(t_n)e^{-j2\pi f t_n}\right|^2 \Big/ N(N-1)\mu \quad (2)$$

to estimate a detectable frequency representation of $x(t)$ from N RSG noisy samples $y(t_n)$'s captured within $\mathcal{T}_r$. It is noted that estimating the signal's exact PSD is not the objective and a frequency representation that enables sensing is sufficient. Tapering function $w(t)$ is used to suppress spectral-leakage where $\mu=\sum_{n=1}^{N_g} w^2(nT_g)$. The standard deviation of a periodogram-type estimator is known to be of the same order as its expected value [10]. To reduce this uncertainly, we average a K number of $X_e(\mathcal{t}_r,f)$ estimates where:

$$\hat{X}_e(f)=\sum_{r=1}^{K} X_e(\mathcal{t}_r,f)/K \quad (3)$$

to enhance the estimation accuracy. This evokes shifting $\mathcal{T}_r$ and the aligning of $w(t)$. Non-overlapping uncorrelated signal windows of length T_0 are considered in this paper.

The sensing technique adopted here comprises two steps: 1) estimating the magnitude spectrum at selected frequency point(s) and 2) comparing the magnitude(s) to pre-set threshold(s). We recall that the signal's exact PSD is not the target. We seek inspecting one frequency point per subband (positioned at its centre) to establish its status i.e. L spectral points are calculated. This can be achieved by performing spectral analysis within a suitably short time windows i.e. low resolution spectrograph. As shown in [8], $T_0\geq 1/B_C$ offers a practical guideline for choosing the analysis window. The sensing problem can be formulated as:

$$\begin{aligned} H_{0,k}:&\quad \hat{X}_e(f_k)<\gamma_k \\ H_{1,k}:&\quad \hat{X}_e(f_k)\geq\gamma_k \qquad k=1,2,\ldots L \end{aligned} \quad (4)$$

where γ_k is the threshold, $H_{0,k}$ hypothesis signifies the absence of an activity in subband k and $H_{1,k}$ exhibits the presence of an activity. Below we show that (3) can deliver reliable spectrum sensing routine provided the adequate selection of the grid density, average sampling rate α and K.

3. STATISTICAL CHARACTERTISCS OF SARS

We present the mean and variance of (3) to assess its adequacy for the MSS pursuit and its accuracy.

3.1 Targeted Frequency Representation

By introducing a random variable c_n which takes a value of "1" if the *n-th* grid point is considered and "0" otherwise where $\Pr\{c_n=1\}=N/N_g$ and $\Pr\{c_n=0\}=(N_g-N)/N_g$, it can be shown that $C(\mathcal{t}_r,f)=E[X_e(\mathcal{t}_r,f)]$ is:

$$C(\mathcal{t}_r,f)=\frac{(N_g-N)P_S(\mathcal{t}_r)+(N_g-1)P_N}{(N-1)N_g f_g}+\frac{E[\mathcal{P}^d(\mathcal{t}_r,f)]}{f_g\mu} \quad (5)$$

, $P_S(\mathcal{t}_r)=\sum_{n=1}^{N_g} E[x^2(nT_g)]w^2(nT_g)/\mu$ is the windowed signal power and $\mathcal{P}^d(\mathcal{t}_r,f)=\left|\sum_{n=1}^{N_g} x(nT_g)w(nT_g)e^{-j2\pi f n T_g}\right|^2$. It can be noticed from (5) that $C(\mathcal{t}_r,f)$ comprises a constant frequency-independent component and the expected value of a discrete-time periodogram [10]. The former would not overshadow any distinctive feature(s) of $E[\mathcal{P}^d(\mathcal{t}_r,f)]$ related to active transmission(s). Below, we show that $E[\mathcal{P}^d(\mathcal{t}_r,f)]$ serves as a detectable spectral component and is independent of $\mathcal{t}_r$ at selected frequency points i.e. f_k's in (4).

Provided that f_g is chosen such that $X_W(f)X_W(f-nf_g)=0$ for $n\neq 0$, $n\in\mathbb{Z}$, where $X_W(\mathcal{t}_r,f)=\int_{t\in\mathcal{T}_r} x(t)w(t)e^{-j2\pi ft}dt$ then:

$E[\mathcal{P}^d(\mathcal{X}_r,f)]=f_g^2\sum_{n\in\mathbb{Z}}E[\mathcal{P}(\mathcal{X}_r,f-nf_g)]$ i.e. avoid aliasing within $\mathcal{B}$ whilst $\mathcal{P}(\mathcal{X}_r,f)=|X_W(\mathcal{X}_r,f)|^2$. Bandpass sampling strategy [3] can be utilised to select f_g. Thus, the adequacy of (2) for the MSS purpose is mandated by $E[\mathcal{P}(\mathcal{X}_r,f)]$. First, let $W(f)=\int_{t\in\mathcal{T}_r}w(t)e^{-j2\pi ft}dt$, $H_m(f)=\int_{-\infty}^{+\infty}h_m(t)e^{-j2\pi ft}dt$, $P_{i,m}(f)=\int_{-\infty}^{+\infty}p_{i,m}(t)e^{-j2\pi ft}dt$, $P_{q,m}(f)=\int_{-\infty}^{+\infty}p_{q,m}(t)e^{-j2\pi ft}dt$, $\hat{P}_{i,m}(f)=H_m(f+f_{C,m})P_{i,m}(f)$, $\breve{P}_{i,m}(f)=H_m(f-f_{C,m})P_{i,m}(f)$, $\hat{P}_{q,m}(f)=H_m(f+f_{C,m})P_{q,m}(f)$, $\breve{P}_{q,m}(f)=H_m(f-f_{C,m})P_{q,m}(f)$. Noting the bandpass nature of $H_m(f)$ over the *m-th* subband and assuming $f_{C,m}>>B_C$, using (1) we obtain:

$$E[\mathcal{P}(\mathcal{X}_r,f)]=0.25\sum_{m=1}^{M}\sigma_{a,m}^2f_{S,m}F_{i,m}(\mathcal{X}_r,f)+\sigma_{b,m}^2f_{S,m}F_{q,m}(\mathcal{X}_r,f) \quad (6)$$

$$F_{i,m}(\mathcal{X}_r,f)=\sum_{n=-\infty}^{+\infty}\Big[\hat{P}_{i,m}(f-f_{C,m})\hat{P}_{i,m}^*(f-f_{C,m}+nf_{S,m}) +\breve{P}_{i,m}(f+f_{C,m})\breve{P}_{i,m}^*(f+f_{C,m}+nf_{S,m})\Big]\otimes\Big[W(f)W^*(f-nf_{S,m})\Big] \quad (7)$$

$$F_{q,m}(\mathcal{X}_r,f)=\sum_{n=-\infty}^{+\infty}\Big[\hat{P}_{q,m}(f-f_{C,m})\hat{P}_{q,m}^*(f-f_{C,m}+nf_{S,m}) +\breve{P}_{q,m}(f+f_{C,m})\breve{P}_{q,m}^*(f+f_{C,m}+nf_{S,m})\Big]\otimes\Big[W(f)W^*(f-nf_{S,m})\Big] \quad (8)$$

. The baud rate is related to the bandwidth $B_{W,m}$ of the baseband shaping filter(s) by: $0.5B_{W,m}<f_{S,m}\le B_{W,m}$ where $B_{W,m}\le B_C$. It implies: $P_{i,m}(f)P_{i,m}(f+nf_{S,m})=0$ and $P_{q,m}(f)P_{q,m}(f+nf_{S,m})=0$ if $n\notin\{-1,0,1\}$. Hence, the components of the summation in (7) and (8) are zero when $n=\pm1$ as the assessed frequency points f_k's in (4) are placed at/near the middle of the subbands i.e. at those frequencies:

$$E[\mathcal{P}(\mathcal{X}_r,f)]= \frac{f_{S,m}}{4}\sum_{m=1}^{M}\sigma_{a,m}{}^2\left\{\left[\left|\hat{P}_{i,m}(f-f_{C,m})\right|^2+\left|\breve{P}_{i,m}(f+f_{C,m})\right|^2\right]\otimes|W(f)|^2\right\} +\sigma_{b,m}{}^2\left\{\left[\left|\hat{P}_{q,m}(f-f_{C,m})\right|^2+\left|\breve{P}_{q,m}(f+f_{C,m})\right|^2\right]\otimes|W(f)|^2\right\} \quad (9)$$

. Therefore, $\mathcal{P}(\mathcal{X}_r,f_k)$ and subsequently $\mathcal{P}^d(\mathcal{X}_r,f_k)$ embodies a distinctive distinguishable feature depicted by the Fourier transform of the transmission filter(s) shaped by the propagation channel and is time-invariant at/near the centre of the subbands. This results in the expected value of (3):

$$\hat{C}(f_k)=\frac{(N_g-N)P_{SA}+(N_g-1)P_N}{(N-1)f_g}+\frac{E[\mathcal{P}^d(\mathcal{X}_r,f_k)]}{f_g\mu} \quad (10)$$

where $P_{SA}=\sum_{r=1}^{K}P_S(\mathcal{X}_r)/K$. Thus, $\hat{X}_e(f_k)$ in (3) is an admissible tool to unveil the presence of an active transmission regardless of the used sampling rate α (a suitable underlying grid density is presumed as described above).

3.2 Estimator's Accuracy

The accuracy of estimation of $\hat{C}(f)$ via (3) can be related to the variance via Chebychev's inequality [8, 9]. We can write: $X_e(\mathcal{X}_r,f)=(N_g-1)T_0\Big[R_{RG}^2(\mathcal{X}_r,f)+I_{RG}^2(\mathcal{X}_r,f)\Big]\Big/N(N-1)\mu$ (11) where the phase shift $\theta(\mathcal{X}_r,f)$ is selected such that each of $R_{RG}(\mathcal{X}_r,f)=\sum_{n=1}^{N}y(t_n)w(t_n)\cos(2\pi ft_n-\theta(\mathcal{X}_r,f))$ and $I_{RG}(\mathcal{X}_r,f)=\sum_{n=1}^{N}y(t_n)w(t_n)\sin(2\pi ft_n-\theta(\mathcal{X}_r,f))$ are uncorrelated for every f. Similar to [9], $X_e(\mathcal{X}_r,f)$ have a chi-square distribution with two degrees of freedom according to Central Limit Theorem (CLT) and $\hat{\sigma}_e^2(f)=\mathrm{var}\{X_e(\mathcal{X}_r,f)\}/K$ can be shown to be closely approximated at f_k's in (4) by:

$$\hat{\sigma}_e^2(f_k)=2\hat{\eta}_kD_k^2/K+2(N_g-N)\big[P_{SA}+\nu P_N\big]D_k\big/[(N-1)f_gK] +(N_g-N)^2\Big[P'_{SA}+2\nu P_{SA}P_N+\nu^2P_N^2\Big]\Big/[(N-1)^2f_g^2K] \quad (12)$$

where $\nu=(N_g-1)/(N_g-N)$, $P'_{SA}=\sum_{r=1}^{K}P_{SA}^2(\mathcal{X}_r)/K$, $0.5\le\hat{\eta}\le1$ and $D_k=E[\mathcal{P}^d(\mathcal{X}_r,f_k)]/f_g\mu$ ($E[\mathcal{P}^d(\mathcal{X}_r,f)]$ is time-invariant at the assessed frequency points). The first component in (12) forms a substantial part of the estimator's variance. Here we show that $\hat{\eta}_k$ can acquire its highest possible value $\hat{\eta}_k=1$ notably degrading the estimation accuracy for certain signals. Note that $\lambda_C(\mathcal{X}_r,f)=E[R^2(\mathcal{X}_r,f)]$ and $\lambda_S(\mathcal{X}_r,f)=E[I^2(\mathcal{X}_r,f)]$ which results in: $\lambda_C(\mathcal{X}_r,f)+\lambda_S(\mathcal{X}_r,f)=E[\mathcal{P}^d(\mathcal{X}_r,f)]$ where $R(\mathcal{X}_r,f)=\sum_{n=1}^{N_g}x(nT_g)w(nT_g)\cos(2\pi fnT_g-\theta(\mathcal{X}_r,f))$ and $I(\mathcal{X}_r,f)=\sum_{n=1}^{N_g}x(nT_g)w(nT_g)\sin(2\pi fnT_g-\theta(\mathcal{X}_r,f))$. Thus,

$$\lambda_C^2(\mathcal{X}_r,f)+\lambda_S^2(\mathcal{X}_r,f)=\eta(\mathcal{X}_r,f)\{E[\mathcal{P}^d(\mathcal{X}_r,f)]\}^2 \quad (13)$$

where $0.5\le\eta(\mathcal{X}_r,f)\le1$ whilst $\hat{\eta}_k$ is the average $\eta(\mathcal{X}_r,f_k)$ along the K signal windows at the f_k frequency point. From (13), it can be seen that $\Gamma(\mathcal{X}_r,f)=\lambda_C(\mathcal{X}_r,f)-\lambda_S(\mathcal{X}_r,f)$ dictates the $\eta(\mathcal{X}_r,f)$ value i.e. if $\lambda_C(\mathcal{X}_r,f_k)\approx\lambda_S(\mathcal{X}_r,f_k)$ we get $\Gamma(\mathcal{X}_r,f_k)\approx0$, $\eta(\mathcal{X}_r,f_k)\approx0.5$ and $\hat{\eta}_k\approx0.5$ which is the case for wide sense stationary signals as in [9]. It can be easily noticed that $\Gamma(\mathcal{X}_r,f)=2\psi(\mathcal{X}_r,f)$. For the legitimate f_g value (see Section 3.1): $P_{i,m}(f)P_{i,m}(f-nf_g)=0$ for $n\ne0$ (n is an integer) and similarly for the quadrate filter(s). Assuming that the analysis window tends to infinity to illustrate the impact of the cyclostationarity on (12) i.e. $W(f)$ tends to a Dirac delta $\delta(f)$, $\psi(\mathcal{X}_r,f)$ is defined by:

$$\psi(\mathcal{X}_r,f)=0.5\cos(2\theta(\mathcal{X}_r,f))f_g^2\sum_{n\in\mathbb{Z}}\sum_{m=1}^{M}G_m(\mathcal{X}_r,f-nf_g) \quad (14)$$

for the M concurrently active subbands where

$$G_m(\mathcal{X}_r,f)=0.125f_{S,m}\Big[\xi_1(f)\sum_{l=-\infty}^{+\infty}\delta(f-f_{C,m}-0.5lf_{S,m}) +\xi_2(f)\sum_{l=-\infty}^{+\infty}\delta(f+f_{C,m}-0.5lf_{S,m})\Big] \quad (15)$$

$$\xi_1(f)=H_m^2(f)\Big[\sigma_{a,m}^2P_{i,m}^2(f-f_{C,m})-\sigma_{b,m}^2P_{q,m}^2(f-f_{C,m})\Big] \quad (16)$$

$$\xi_2(f)=H_m^2(f)\Big[\sigma_{a,m}^2P_{i,m}^2(f+f_{C,m})-\sigma_{b,m}^2P_{q,m}^2(f+f_{C,m})\Big]. \quad (17)$$

Formulas (14)-(17) show that $\psi(\mathcal{X}_r,f)$ can have nonzero values concentrated at frequencies equal to multiples of half of the symbol rate $f_{S,m}$ and belong to the *m-th* active subband. Such peaks are experienced when any mismatch between $\sigma_{a,m}^2P_{i,m}(f)$ and $\sigma_{b,m}^2P_{q,m}(f)$ takes place generating discrepancies between $\lambda_R(\mathcal{X}_r,f)$ and $\lambda_I(\mathcal{X}_r,f)$. This yields abrupt surges in the estimation variance at the corresponding frequencies according to (12) and (13). This phenomenon is

clearly observed with BPSK signals where only an inphase branch is present. Thus $\eta(\mathcal{I}_r, f_k)$ and subsequently $\hat{\eta}_k$ can tend to their maximum values causing noticeable deterioration in the estimator's accuracy in case f_k falls at/near the $f_n = 0.5nf_{S,m}$ frequency(ies) that belong(s) to the m-th active transmission band. Whilst for QAM and QPSK, typically $\sigma^2_{a,m}P_{i,m}(f) = \sigma^2_{b,m}P_{q,m}(f)$ i.e. $\psi(\mathcal{I}_r, f) \approx 0$ and $\hat{\eta}_k = 0.5$ is commensurate. If no beforehand knowledge is available on the modulation scheme characteristics, $\hat{\eta}_k = 1$ should be selected to avoid any unforeseen anomalies in the estimator's performance. Therefore, the accuracy of (3) can be affected by the signal's cyclostationarity and any processing task that relies on the spectral analysis, e.g. MSS, should consider such aspect. The accuracy of the above analysis was verified through numerical examples (not shown here).

4. RELIABLE SPECTRUM SENSING

The reliability of a sensing technique is reflected by its ability to meet a sought system behaviour that is commonly expressed by the Receiver's Operating Characteristic(ROC) [1]. Here, we procure the reliability recommendations to ensure that the proposed method satisfies the sought ROC probabilities of a targeted subband indexed by k in the sequel.

4.1 Reliability Recommendations

According to CLT, $\hat{X}_e(f)$ can be approximated by a normal distribution at every f for large K (in practice $K \geq 20$ suffices[1]). This is validated below by simulations even for $K < 20$. Thus, (3) can be compactly written as: $\hat{X}_e(f_k) \sim \mathcal{N}(m_{0,k}, \sigma^2_{0,k})$, $m_{0,k} = \tilde{C}(f_k)$ and $\sigma_{0,k} = \hat{\sigma}_e(f_k)$ for $H_{0,k}$ and similarly $\hat{X}_e(f_k) \sim \mathcal{N}(m_{1,k}, \sigma^2_{1,k})$ for $H_{1,k}$. From (4), the probability of a false alarm in the k-th subband is:

$$P_{f,k}(\gamma_k) = \Pr\{H_{1,k} \,|\, H_{0,k}\} = Q[(\gamma_k - m_{0,k})/\sigma_{0,k}] \quad (18)$$

and that of correct detection is:

$$P_{d,k}(\gamma_k) = \Pr\{H_{1,k} \,|\, H_{1,k}\} = Q[(\gamma_k - m_{1,K})/\sigma_{1,k}] \quad (19)$$

for a preselected threshold value γ_k where $Q(z)$ is the tail probability of normal distribution. In practice, the user typically specifies: $P_{f,k} \leq \Delta$ and $P_{d,k} \geq \ell$. From (18) and (19):

$$\gamma_{\min,k} \leq \gamma_k \leq \gamma_{\max,k} \quad (20)$$

$\gamma_{\min,k} = m_{0,k} + Q^{-1}(\Delta)\sigma_{0,k}$, $\gamma_{\max,k} = m_{1,k} + Q^{-1}(\ell)\sigma_{1,k}(f_k)$ and

$$m_{1,k} - m_{0,k} \geq Q^{-1}(\Delta)\sigma_{0,k} - Q^{-1}(\ell)\sigma_{1,k} \quad (21)$$

which defines the reliability condition of the MSS. The mean and standard deviation values in (18) and (21) can be directly obtained from (10) and (12) respectively. Adopting a conservative approach, it can be shown that (21) produces:

$$K \geq \left\{Q^{-1}(\Delta)\tilde{K} - Q^{-1}(\ell)\sqrt{\tilde{K}^2 + 2\tilde{K} + 2\hat{\eta}_k}\right\}^2, \quad (22)$$

$\tilde{K} = 2B_C\phi_k N(N_g - N)\left[1 + (N_g - 1)SNR^{-1}/(N_g - N)\right]/N_g\alpha(N-1)$ and $SNR = P_{SA}/P_N$. Whilst, $\phi_k = P_{SA}/P_{SA,k}$ is the ratio of the total signal power to that occupying the targeted subband.

Formula (22) is a conservative lower bound on the number of needed window averages to fulfil the pursed detection probabilities. It is a function of the average sampling rate, signal to noise ratio, the active subbands power ratios and the uniform grid density. The recommendation demonstrates the trade-offs between the number of estimate averages and the deployed sampling rate in a particular scenario. It can be used to decide on the average sampling rate for a number of estimate averages possibly demanded by practical constraints such as latency in a continuous processing environment. The impact of the nonstationary nature of the processed signals is manifest by $\hat{\eta}_k$ (see Section 3). Formula (22) affirms that the sensing task can be accomplished with arbitrarily low sampling rates at the expense of longer signal observation windows. A numerical example is presented below to verify its accuracy. If more than one subband is targeted, the user should survey their individual α / K requirements via (22). Aiming to detect a weak or high performance subband(s) would request more K and/or higher α compared to a stronger or lower performance ones. The thresholds needed in (4) for each subband is set by (20).

The spectral peaks D_n's for $n = 1, 2, \ldots L$ can be learnt a priori when the transmissions are known to be present as in [1, 2]. Such knowledge can be exploited to determine ϕ_k and the parameters needed for calculating the thresholds in (20) e.g. for the severe cases when the maximum expected subbands activity is incurred. Correlated and/or overlapping signal windows can be easily incorporated into the analysis above by using existing results in the literature on variance reductions e.g. Welch periodograms [10]. Cooperation among a number of possible sensing devices can be implemented at a network level higher than the studied physical level.

4.2 RSG versus TRS and Uniform Sampling

RSG becomes identical to TRS as the underlying grid rate tends to infinity, and (22) emerges as:

$$K_{TRS} \geq \left\{Q^{-1}(\Delta)\tilde{K}_{TRS} - Q^{-1}(\ell)\sqrt{\tilde{K}^2_{TRS} + 2\tilde{K}_{TRS} + 2\hat{\eta}_k}\right\}^2 \quad (23)$$

where $\tilde{K}_{TRS} = 2B_C\phi_k N[1 + SNR^{-1}]/(N-1)\alpha$. Whilst, the scheme becomes uniform sampling when all the grid points are considered and the recommendation reduces to:

$$K_{US} \geq \left\{Q^{-1}(\Delta)\tilde{K}_{US} - Q^{-1}(\ell)\sqrt{\tilde{K}^2_{US} + 2\tilde{K}_{US} + 2\hat{\eta}_k}\right\}^2 \quad (24)$$

where $\tilde{K}_{US} = 2B_C\phi_k SNR^{-1}/f_{US}$ and f_{US} is the uniform sampling rate that is appropriately set to avoid aliasing within $\mathcal{B}$. Comparing RSG and TRS, it can be shown that $K < K_{TRS}$ for a reasonable f_g. Formulas (22)-(24) offer a means to evaluate the requirements of each of their corresponding sampling scheme and assess the benefits/complexity of SARS with RSG. They can be used to examine the number of needed signal samples of each of the schemes. This can be a crucial factor as the adopted MSS involves discrete-time Fourier transform or an optimized version. Unlike TRS and Poisson sampling, RSG maintains a minimum distance between the collected samples i.e. T_g and is better suited for FFT-like algorithms e.g. zero filling of unused grid points [6].

5. SIMULATIONS

Consider a multiband system comprising $L = 40$ contiguous subbands where $B_C = 2.5$ MHz and they are located in $\mathcal{B} = [1.65, 1.75]$ GHz. QAM signals are transmitted over the active subbands (i.e. $\hat{\eta}_k = 0.5$) noting that the SNR is 1.6 dB. The grid rate $f_g = 220$ MHz which satisfies $X_W(f)X_W(f - nf_g) = 0$ if $n \neq 0$ (n is an integer) is used along with a Blackman window of length $T_0 = 1\,u$s. A sampling rate $\alpha = 68$ MHz is decided, it is significantly lower than the minimum valid uniform sampling rate i.e. 220 MHz. The aim is to fulfil the detection requirements of the targeted subband centred at f_{31}. The user specified: $P_{f,31}(\gamma_{31}) \leq 0.05$ and $P_{d,31}(\gamma_{31}) \geq 0.96$. For $\phi_{31} = 2.12$ (four simultaneously active subbands), $K \geq 11$ estimates need to be averaged in (3) to meet the sought system performance according to (22) . In Fig. 1a, we show the ROC of SARS with RSG method for a threshold sweep and in Fig. 1b the probabilities are displayed for the threshold values in (20). The results were obtained from 10000 independent simulations.

Fig. 1 confirms the moderately conservative nature of the given reliability recommendations where the desired performance is achieved for $K \geq 11$ upon satisfying the inequality in (21). This also affirms that the assumptions undertaken did not have noticeable effect on the accuracy of results including the normality one. Thus, the proposed technique here provides nearly 67% saving on the sampling rate and 20% reduction on the number of processed samples in comparison to uniform sampling. It also gives nearly 20% saving on the latter compared to TRS. It is clear that SARS with RSG delivers notable savings in terms of the complexity of the sensing procedure, especially in low spectrum occupancy environment e.g. CR in certain frequency ranges. Formulas (22)-(24) allow the user to examine the possible benefits of utilizing SARS in a given scenario. For illustration purposes, Fig. 2 depicts the targeted subband's ROC if the present transmissions were of a BPSK type and $\hat{\eta}_{31} = 0.5$ i.e. the cyclostationarity effect(s) on the estimation accuracy is ignored. It is clear from the figure that the detection method has failed to deliver the requested probabilities for $K = 11$. This demonstrates the impact of the nonstationarity of communication signals on SARS and that precautions should be taken. If we chose $\hat{\eta}_k = 1$ in (22), we would attain $K \geq 15$ which mends the MSS response (see Fig. 2).

6. CONCLUSIONS

The proposed SARS with RSG is a reliable spectrum sensing technique that offers substantial savings on the sampling rate compared to the uniform-sampling-based ones. It can use considerably low sampling rates i.e. ease the stringent sampling requirements of the wideband MSS procedure. The cyclostationary nature of communication signals is shown to cause degradation in the SARS quality and should be countered. The provided reliability guidelines, which ensure fulfilling the detection probabilities, illustrate the trade-offs between the sampling rate and the length of the observation window. This paper serves as an impetus and prompts further research into DASP-based MSS methods.

REFERENCES

[1] Z. Quan, S. Cui, H. V. Poor, and A. H. Sayed, "Collaborative Wideband Sensing for Cognitive Radios," *IEEE Signal Processing Magazine*, vol.25, pp.60-73, 2008.

[2] J. Ma, G. Y. Li, and B. H. Juang, "Signal processing in cognitive radio," *Proceedings of the IEEE*, vol.97, pp.805-823, 2009.

[3] R. Vaughan, N. Scott, and D. White, "The Theory of Bandpass Sampling," *IEEE Trans. on Sig. Proces*, pp.1973-1984, 1991.

[4] Y. Polo, Y. Wang, Pandharipande, and G. Leus, "Compressive Wide-band Spectrum Sensing," *in proc.IEEE Int. Conf. on Acous., Speech and Sig. Proces.*, 2009, TX, pp.2337-2340.

[5] M. Mishali and Y. C. Eldar, "Blind Multiband Signal Reconstruction: Compressed Sensing For Analog Signals," *IEEE Trans. on Signal Process.*, vol.57, pp.993-1009, 2009.

[6] I. Bilinskis, Digital Alias-free Signal Processing, New York, John Wiley and Sons, 2007.

[7] R. Venkataramani and Y. Bresler, "Perfect Reconstruction Formulas and Bounds on Aliasing Error in Sub-Nyquist Nonuniform sampling of Multiband Signals," *IEEE Trans. On Info. Theory*, vol.46, pp.2173-2183, 2000.

[8] B. I. Ahmad and A. Tarczynski, "Reliable Wideband Multichannel Spectrum Sensing Using Randomized Sampling Schemes," *Signal Processing*, vol.90, pp.2232-2242, 2010.

[9] B. I. Ahmad and A. Tarczynski, "Wideband Spectrum Sensing Technique Based on Random Sampling on Grid: Achieving Lower Sampling Rates," *Digital Signal Processing,* 2011.

[10]M. H. Hayes, Statistical Digital Signal Processing and Model ing, John Wiley & Sons, 1996.

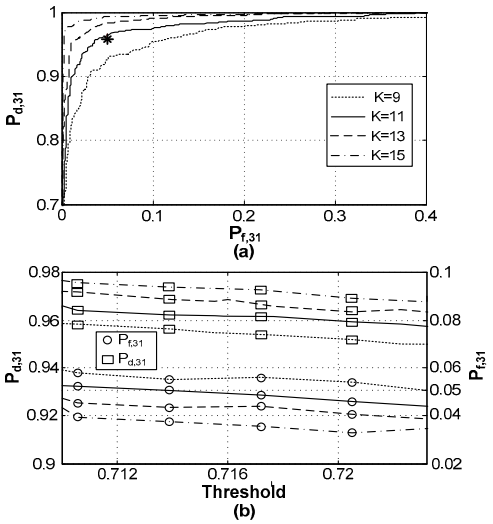

Fig. 1, Detection probabilities of the targeted subband. (a) ROC for a threshold sweep; asterisk is $(0.05, 0.96)$, (b) $\gamma_{\min,31} \leq \gamma_{31} \leq \gamma_{\max,31}$.

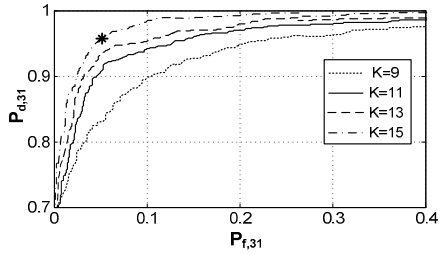

Fig. 2, ROC for the BPSK case; asterisk $(0.05, 0.96)$.